Auto-resonant Control of the H-Bridge Resonant Converter for Inductive Power Transfer Applications

Grazian, Francesca; van Duijsen, Peter; Roodenburg, Bart; Soeiro, Thiago Batista; Bauer, Pavol

DOI
10.1109/ISIE45063.2020.9152592

Publication date
2020

Document Version
Accepted author manuscript

Published in
2020 IEEE 29th International Symposium on Industrial Electronics, ISIE 2020 - Proceedings

Auto-resonant Control of the H-Bridge Resonant Converter for Inductive Power Transfer Applications

Francesca Grazian, Peter van Duijsen, Bart Roodenburg, Thiago Batista Soeiro, and Pavol Bauer
Electrical Sustainable Energy Department
Delft University of Technology, Delft 2628 CD, The Netherlands
Email: (F.Grazian, P.J.vanDuijsen, B.Roodenburg, T.BatistaSoeiro, P.Bauer)@tudelft.nl

***Abstract*—In inductive power transfer applications that use resonant compensation networks, the commonly employed H-bridge inverter should be kept operating in soft-switching to ensure high power efficiency and low irradiated electromagnetic noise. To achieve so, the zero-crossing detection circuit for the resonant current or voltage must be fast and accurate in any operating condition. This paper researches the concept of an auto-resonant control for the typical H-bridge resonant converter used in wireless charging systems. In the method proposed here, the reference levels for the zero-crossing detection of the inverter's current are automatically adapted depending on the slope of the current itself at the zero-crossing. In this way, it is possible to compensate for the circuit delay even in the presence of parameters' variation and to ensure that the soft-switching is always maintained. The functionality of this control method is proven first mathematically, and then with circuit simulations. The core steps for the implementation are described with the support of functional blocks. Finally, the system start-up strategy is explained, which uses an auxiliary timed oscillator to modulate the inverter with a fixed 50% duty cycle at a higher frequency than the nominal. This guarantees that the start-up is in the inductive region and, thus, the zero-voltage switching turn-on. Once the detection circuits sense the current flow, the oscillator is automatically disabled, and the nominal power transfer starts.**

***Index Terms*—Control, inductive power transfer, inverter, soft-switching, wireless charging, zero voltage switching.**

I. Introduction

Over the last decade, wireless charging of electric vehicles (EVs) has been gaining popularity because, in some specific applications, it has clear advantages with respect to the traditional charging through cable. For example, wireless charging is convenient in dynamic charging and to charge autonomous-driven EVs. To make this technology competitive, the power transfer efficiency from the source to the EV battery needs to be maximized, and that can be achieved by minimizing the power losses of each power conversion stage.

The most used method in EV wireless charging is inductive power transfer (IPT) that uses magnetic resonant coupling. Thereby, the power is transferred from the transmitter to the receiver coil through an $85\,\mathrm{kHz}$ magnetic field [1]. This magnetic field is generated by a time-varying current that flows in the transmitter coil which, in turn, is produced by an inverter. In EV wireless charging applications, the most used inverter topology is the full- or H-bridge converter that is composed of four switching units, as shown in Fig. 1. In the H-bridge inverter, there are two main sources of power losses: the conduction and the switching losses. For a certain input

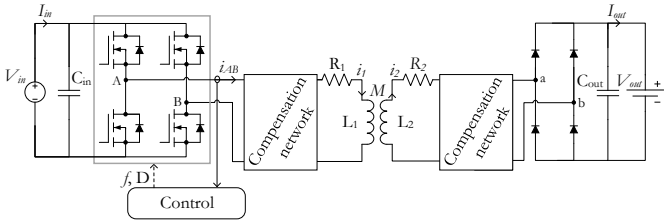

Fig. 1. General circuit used in EV wireless charging.

voltage and power level, the conduction losses can be limited by choosing unipolar switches, such as MOSFETs, with low on-state resistance. This choice generally leads to higher costs because it may require large areas of the semiconductor chip. On the other hand, the switching losses can be suppressed by operating the inverter in a soft-switching condition. Especially while employing Silicon MOSFETs, the turn-on transition at the zero-voltage switching (ZVS) needs to be ensured to discharge the drain-source capacitance of the switches and to avoid the reverse recovery of the anti-parallel diodes. As explained in [2]–[6], it is possible to achieve the ZVS turn-on in all inverter's active semiconductors when the resonant current lags the generated square-wave voltage, i.e. when the system operates in the inductive region. This means that the H-bridge inverter has to be modulated at a switching frequency slightly higher than the natural frequency of the passive compensation network. This can be realized by switching the inverter's legs just before the resonant current's zero-crossing. Therefore, the zero-crossing detection of the resonant current is a fundamental part of the H-bridge inverter's control loop.

There are some factors that make the current's zero-crossing detection challenging. The accuracy and precision of the zero-crossing detection should be relatively high in the inverter's operating frequency range 79-$90\,\mathrm{kHz}$ defined by [1], [7]. Moreover, due to manufacturing tolerances, temperature rise, drop of magnetic core permeability, or degradation, the components of the resonant circuit might assume sightly different values from the theoretical design. In those cases, the actual resonant frequency would change and, to maximize the power transfer efficiency, the operating frequency needs to be re-tuned within the allowed frequency range. Additionally, in EV wireless charging applications, the operating condition is not fixed because there are two important parameters that can vary. The first parameter is the coupling factor between the transmitter and receiver coils, which strongly depends on their

TABLE I
EXAMPLE OF DELAYS INTRODUCED BY ICS AND THE GATE DRIVER.

Component		Delay (ns)[1]	
Type	Name	Δt_{on}	Δt_{off}
Operational amplifier	TL071	100	100
Differential comparator	LM211	115	165
Gate driver	IR 2110	120	94
	Total	335	359

[1] From the datasheet

alignment. The other parameter is the equivalent output load that changes while the EV battery is being charged. The zero-crossing detection must be fast and adaptable in order to keep the ZVS turn-on at any operating condition.

In the literature, different current's zero-crossing detection circuits can be found. The need for a fast inverter control loop to detect the zero-crossing accurately is already acknowledged in [8]–[11]. In [8], [9] and [11], the inverter's control has been implemented by combining analog electronics with an FPGA because of the required fast processing speed. Another alternative widely used is the phase-locked loop (PLL). However, the detection of the zero-crossing must be precise, and analog-to-digital converters (ADCs) generally do not have enough resolution for these relatively high frequencies. To overcome this problem, analog current measurements are typically used followed by a comparator that performs the detection. Since the detection and the conditioning circuit themselves introduce a fixed time delay, it is important to take it into account in the implementation. In [10], the time delay is compensated by setting a manually adjustable reference to the comparator that depends on the measured current peak. However, in a real application, this reference needs to be adjusted automatically.

This paper describes the concept of an auto-resonant control for the H-bridge inverter used in inductive power transfer applications. This concept consists of adapting the reference levels of the current's zero-crossing detection depending on the slope of the current at the zero-crossing. In this way, the operation is always adjusted to be close to the actual resonant frequency of the circuit while ensuring the ZVS turn-on of the inverter. The general features and the analysis of the current's zero-crossing detection are explained in Section II. The proposed concept of the auto-resonant current's zero-crossing detection is described in Section III. Since this control concept has an analog implementation, the start-up of the power transfer is critical. The start-up strategy is addressed and explained in Section IV, and it has been validated in combination with the auto-resonant control through circuit simulations. Finally, conclusions on the concept of the auto-resonant control are described in Section V.

II. CURRENT'S ZERO-CROSSING DETECTION

A general circuit schematic of a wireless charging system is shown in Fig. 1. The inverter's control loop takes as input the measurement of the resonant current $i_{AB} = i_{AB}(t)$, and it gives as output the operating frequency and duty cycle to the switches' gate driver. Ideally, the zero-crossing of i_{AB} could be detected by comparing the measured current waveform to

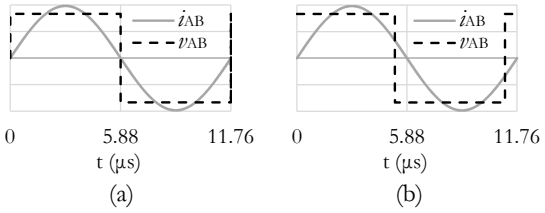

Fig. 2. Inverter voltage v_{AB} and current i_{AB} at: (a) ZCS, (b) ZVS operation.

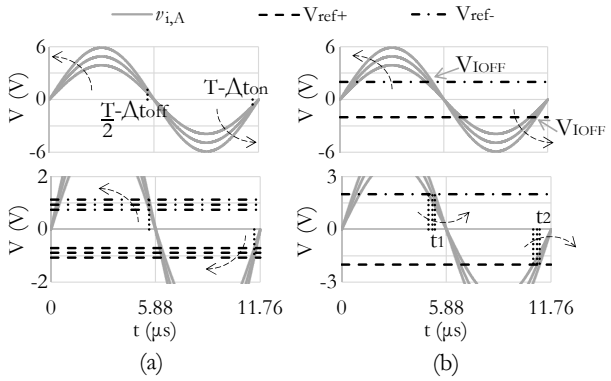

Fig. 3. Voltage signal of the sensed resonant current, $v_{i,A}$, and the reference voltages V_{ref+}, V_{ref-} for: (a) compensating the delays times Δt_{on}, Δt_{off} introduced by the analog circuits ($T=\frac{1}{f}$), (b) detecting the current I_{OFF} which guarantees ZVS turn-on.

0 V (ground reference voltage). An example of inverter ZCS operation is shown in Fig. 2(a) for the operating frequency of 85 kHz. However, in a real circuit, all the integrated circuits (ICs), analog logics and the gate drivers introduce a time delay Δt in the control signal, which would make the commutation happen at a different current. After the current measurement, the zero-crossing detection circuit comprises of at least one operational amplifier (opamp) to perform the signal conditioning and one differential comparator to realize the detection. For example, Table I shows the typical delay times caused by the commercial opamp TL071, the differential comparator LM211 and the gate driver IR2110. Considering i_{AB} to be a 85 kHz sinusoidal current with an amplitude of 6 A, the actual inverter's switching current can be calculated by using (1), where I is the current's root mean square. As a result, the total delay in Table I would make the inverter switching at about 1 A instead of at the zero-crossing. Therefore, if the ground potential is considered as the reference for the comparator (V_{ref}=0 V), the inverter would operate in hard-switching.

$$i_{AB} = i_{AB}(t) = \sqrt{2}I\sin(2\pi ft) = \sqrt{2}I\sin(\omega t) \qquad (1)$$

Given a control circuit, Δt can be considered to be constant during the operation, and it is possible to compensate for the delay Δt, by imposing $V_{ref} \neq 0$ V. However, both the amplitude and the frequency of i_{AB} might vary depending on the operating condition and the circuit parameters' variation. As a consequence, even though the Δt is nearly constant, the value of V_{ref} that compensates for Δt varies in different operating conditions. To prove this, let's still consider that i_{AB} is an 85 kHz sinusoidal current. Fig. 3 shows the voltage measured signal $v_{i,A}$ equivalent to the current i_{AB} after the

signal conditioning stage which result in a 85 kHz sinusoidal voltage with 1:1 amplitude ratio with respect to the original current i_{AB}, and the voltage references V_{ref+} and V_{ref-} for the zero-crossing detection of i_{AB} at the positive and negative slope, respectively. In this example, the amplitude of i_{AB} is assumed to vary in the range of 4-6 A. To compensate for the constant delays Δt_{on}, Δt_{off} in Table I, Fig. 3(a) shows that the value of V_{ref} might vary considerably when the amplitude of i_{AB} varies. The variation of V_{ref} would be even more accentuated if the operating frequency also changes. This means that, to achieve an accurate zero-crossing detection, the reference V_{ref} must be adjusted during the operation. At this point, it is interesting to compute the mathematical expression of V_{ref} to verify what observed in Fig. 3(a).

The expression of i_{AB} in (1) can be rewritten in terms of the voltage signal representing the measured current $v_{i,A}$ as shown in (2). Moreover, since the time instants $\frac{T}{2} - \Delta t_{on}$ and $T - \Delta t_{off}$ in Fig. 3(a) are close to the current's zero-crossings, the small-angle approximation in (3) can be considered to be valid. By using this approximation, (2) simplifies in (4).

$$v_{i,A}(t) = \sqrt{2} V_{i,A} \sin(\omega t) \tag{2}$$

$$-\frac{\pi}{6} < \omega t < \frac{\pi}{6} \quad \rightarrow \quad \sin(\omega t) \approx \omega t \tag{3}$$

$$v_{i,A}(t) = \sqrt{2} V_{i,A} \sin(\omega t) \approx \sqrt{2} V_{i,A} \omega t \tag{4}$$

The value of V_{ref+}, V_{ref-} can be computed as described in (5), (6), respectively. By observing the small-angle approximation of V_{ref+} and V_{ref-}, it is possible to notice that their first term is equal to the approximated time-derivative of $v_{i,A}$ in (7). By combining (5) and (6) with (7), it can be concluded that, according to the small-angle approximation in (3), V_{ref+} and V_{ref-} are equivalent to (8) and (9), respectively. This means that the references V_{ref+}, V_{ref-} depend on the slope of $i_{AB}(t)$ during the zero-crossing.

$$V_{ref+} = \sqrt{2} V_{i,A} \sin(\omega \Delta t_{on}) \approx \sqrt{2} V_{i,A} \omega \Delta t_{on} \tag{5}$$

$$V_{ref-} = \sqrt{2} V_{i,A} \sin(\omega \Delta t_{off}) \approx \sqrt{2} V_{i,A} \omega \Delta t_{off} \tag{6}$$

$$\frac{d}{dt} v_{i,A}(t) \approx \sqrt{2} V_{i,A} \omega \tag{7}$$

$$V_{ref+} \approx \frac{d}{dt} v_{i,A}(t) \Delta t_{on} \tag{8}$$

$$V_{ref-} \approx \frac{d}{dt} v_{i,A}(t) \Delta t_{off} \tag{9}$$

If both the amplitude and frequency of $i_{AB}(t)$ are constant, the delays Δt_{on} and Δt_{off} could be compensated by choosing fixed values for V_{ref+} and V_{ref-}. On the other hand, if the operating frequency is fixed, V_{ref+} and V_{ref-} would depend only on the amplitude of i_{AB}. In that case, the approach in [10] could be used which adjusts V_{ref+} and V_{ref-} by measuring the amplitude of i_{AB}. However, since the allowed frequency range for the EV wireless charging is 79-90 kHz, the operating frequency can be fine-tuned to match the actual resonant frequency of the circuit that can differ due to components' variations. This means that, for the same current amplitude, the slope at the zero-crossing could be different depending on the period's duration. Therefore, it is chosen to adjust V_{ref+} and V_{ref-} based on the $\frac{d}{dt} i_{AB}$ at the zero-crossing of i_{AB}.

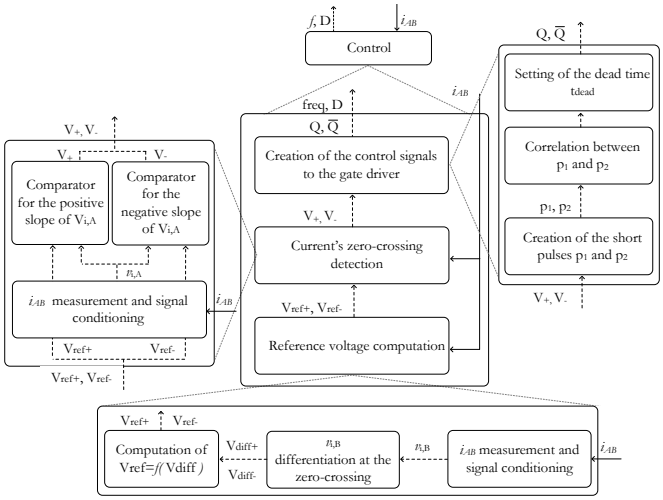

Fig. 4. Block diagram of the auto-resonant control's concept.

To achieved the soft-switching operation, the ZVS turn-on of the inverter must be ensured. This can be done by switching the inverter's legs before the zero-crossing of i_{AB} as shown in Fig. 2(b). In particular, [2]–[6] define the minimum current I_{OFF} that ensures the ZVS turn-on. By considering the same measured current signal $v_{i,A}$, and assuming that $V_{I_{OFF}}$ corresponds to the measurement of I_{OFF}, theoretically the ZVS turn-on is achieved when the references V_{ref+}, V_{ref-} are equal to $V_{I_{OFF}}$ as shown in Fig. 3(b), where $I_{OFF} = 2$ A. According to [2]–[6], the value of I_{OFF} depends on the MOSFET's drain-source blocking voltage $V_{ds,off}$, drain-source capacitance C_{ds} and the half-bridge switching dead time t_{dead}. This means that, for the same MOSFET, DC input voltage V_{in}, and t_{dead}, the value of I_{OFF} can be considered to be constant. According to Fig. 3(b), the I_{OFF} detection instants t_1 and t_2 would vary if either the amplitude or the frequency of i_{AB} changes. However, the comparators would follow this change and detect I_{OFF} by keeping V_{ref+} and V_{ref-} constant at $V_{I_{OFF}}$. Therefore, for the same I_{OFF}, the references V_{ref+} and V_{ref-} do not have to be adjusted to keep the ZVS turn-on at different operating conditions.

III. Concept of the Auto-Resonant Control

The concept of the auto-resonant control has been derived from the mathematical analysis in Section II, and it is summarized by the block diagram in Fig. 4. The auto-resonant control can be used with H-bridge inverters likewise in Fig. 1, and it can work with any resonant compensation network as long as the inverter's current approximates a sinusoid. The key element in this control is that the current's zero-crossing detection uses the adjustable references V_{ref+} and V_{ref-} such that the ZVS turn-on is kept at different operating conditions. The value of V_{ref+} and V_{ref-} depends on two terms: the delay times Δt_{on}, Δt_{off} introduced by the control circuit, and the detection voltage $V_{I_{OFF}}$ equivalent to I_{OFF}. The first term is adjusted depending on the slope of i_{AB} at the zero crossing, according to (8) and (9). On the other hand, if I_{OFF} is fixed, the second

term is also fixed. The two different reference voltages V_{ref+} and V_{ref-} are computed separately to detect more accurately the zero-crossing of i_{AB} for the positive slope ($\frac{d}{dt}i_{AB}>0$) and negative slope ($\frac{d}{dt}i_{AB}<0$) of i_{AB}, respectively. This choice has been made because it might exist an asymmetry between the on- and off-reaction time of the components, as it can be noticed from the delays in Table I. This approach also takes into account the potential difference between the positive and negative half-wave of i_{AB}, which can be due to the fact that the resonant oscillations are not perfectly sinusoidal.

Fig. 5(a) shows the measured current signal $v_{i,A}$ with the updated references V_{ref+}, V_{ref-} that are composed of the two terms explained above. This means that V_{ref+} and V_{ref-} in Fig. 5(a) correspond to the updated time instants $t_1 + \Delta t_{off}$ and $t_2 + \Delta t_{off}$ which differ to the ones in Fig. 3.

The auto-resonant control is composed of three main blocks as shown in Fig. 4. The first block computes the adjusted reference voltages V_{ref+} and V_{ref-}, and it is explained in Section III-A. The second block performs the current's zero-crossing detection, and it is described in Section III-B. Finally, the third block creates the suitable control signals for the switches' gate driver, and it is discussed in Section III-C.

A. Reference voltage computation block

This first block can be divided into three main parts, as shown in Fig. 4. First, the inverter's current i_{AB} is measured and, after a signal conditioning stage, the measured current $V_{i,B}$ is generated. Then, the measured $V_{i,B}$ is differentiated at both the positive and negative zero-crossings. The rectified values of both differentiation produce the voltages V_{diff+} and V_{diff-} for the positive and negative slope, respectively. Finally, the adjusted reference voltages V_{ref+} and V_{ref-} are computed as function of V_{diff+} and V_{diff-}, respectively. Fig. 5(a) shows a qualitative representation of V_{ref+} and V_{ref-}.

B. Current's zero-crossing detection block

This second block can be divided into two main parts, as shown in Fig. 4. First, i_{AB} is measured. Then, the conditioned measurement $V_{i,A}$ is used as main input for two different comparators. Additionally, the comparator for the positive slope's zero-crossing takes as inverting input the reference voltage V_{ref+}, while the comparator for the negative slope's zero-crossing takes as non-inverting input the reference voltage V_{ref-}. In this way, the positive and negative slopes are treated separately. Each comparator gives a high output (+5 V) when $V_{i,A}$ is greater than the reference, and low output (0 V) otherwise. As a result, the outputs are the two square waves V_+ and V_- produced by the comparators, which might overlap because they are completely independent of each other. The outputs V_+ and V_- are qualitatively shown in Fig. 5(b).

C. Creation of the control signals to the gate driver block

This third block can be divided into three main parts, as shown in Fig. 4. Since the signals V_+ and V_- coming from the comparators might overlap, they need to be related to each other such that the control signal to the gate driver is unique. According to Section III-B, V_+ is the control signal related to the positive slope zero-crossing of i_{AB}, while V_- is related to the negative slope zero-crossing of i_{AB}. This means that the part of interest of V_+ and V_- is just the one related to their rising edge. Therefore, to guarantee that there is no overlap, V_+ and V_- are shorten into the short pulses p_1 and p_2 which only focus on their parts of interest. The qualitative representation of p_1 and p_2 is shown in Fig. 5(c). After this, the intervals of time in which p_1 and p_2 assume the high value are again extended, such that each signal switches to low as soon as the other one becomes high. In this way, it is possible to make sure that the control signals coming from the positive

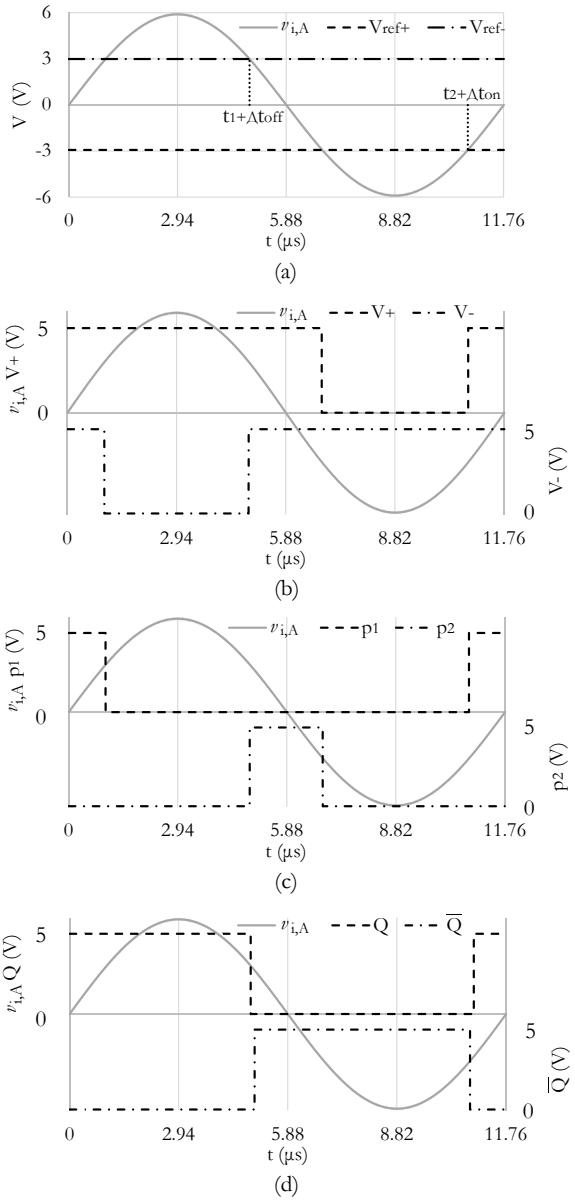

Fig. 5. Qualitative waveforms of the auto-resonant control that refer to the block diagram in Fig. 4. (a) Voltage signal of the measured current $v_{i,A}$ and the reference voltages V_{ref+}, V_{ref-} for detecting the current I_{OFF} which guarantees ZVS operation (as in Fig. 2(b)) and that also takes into account the circuit's delay times Δt_{on}, Δt_{off}. (b) Comparators' output voltages V_+, V_-. (c) Short pulses p_1, p_2. (d) Output voltages Q, $\overline{Q}$ to the gate driver.

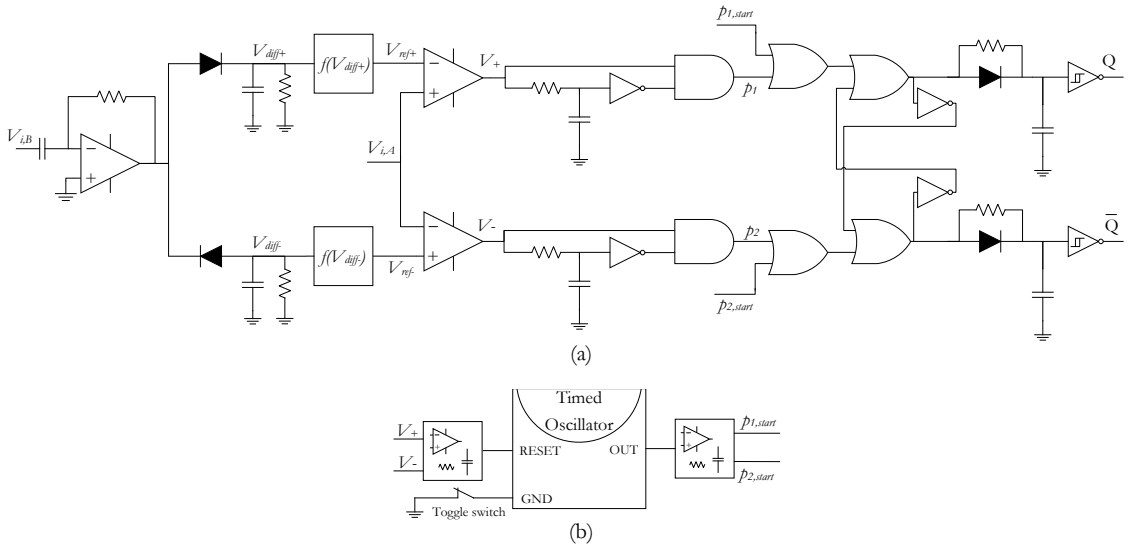

Fig. 6. Summarized circuit schematic used to simulate: (a) the auto-resonant control concept with (b) the start-up strategy.

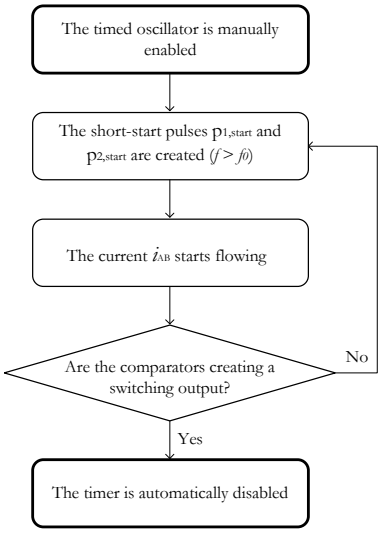

Fig. 7. Flow chart of the start-up strategy used in the auto-resonant control.

and the negative slope of i_{AB} are not overlapping. Finally, the last step consists in setting the optimal dead time t_{dead} because, as explained in [6], it is important that t_{dead} is long enough to ensure the actual ZVS turn-on. At this point, the gating control signals Q and $\overline{Q}$ are created, and they are sent to the gate driver. The qualitative representation of Q and $\overline{Q}$ is shown in Fig. 5(d). The control signal Q becomes high in correspondence of the positive-slope zero-crossing of i_{AB}. This means that, among the switches in Fig. 1, Q1 and Q4 are conducting when Q is high, while Q2 and Q3 are open. The complementary operation is valid for the control signal $\overline{Q}$.

IV. Start-up strategy

The concept of the auto-resonant control explained in Section III can be implemented by using only analog components, as shown in Fig. 6(a). The analog implementation complicates the start-up of the power transfer because, when i_{AB} is zero, the comparators will not work. Therefore, to start the power transfer, the circuit needs to excite the flow of I_{AB}.

The designed start-up strategy uses a timed oscillator, as shown in Fig. 6(b). To start the wireless charging process, the timed oscillator is manually enabled by connecting the oscillator's ground pin (GND), that is initially floating, to the ground reference voltage. After this, the generation of the starting short pulses $p_{1,start}$ and $p_{2,start}$ begins which substitute the nominal short pulses p_1 and p_1 during the start-up. The frequency of this initial pulses is higher than the nominal to ensure that the operation is in the inductive region. As a result, during the start-up, the control signals to the gate driver Q and $\overline{Q}$ have higher frequency than the nominal. The current i_{AB} starts building up in the inverter and, once its amplitude is high enough, the comparators starts generating the output voltages V_+ and V_-. As soon as the comparators start working, the oscillator is automatically disabled through its RESET pin, which voltage is changed from high to low (from $5\,\mathrm{V}$ to $0\,\mathrm{V}$). At this point, $p_{1,start}$ and $p_{2,start}$ stop, and p_1 and p_2 start driving the outputs Q and $\overline{Q}$. This start-up strategy is summarized in the flow chart of Fig. 7.

The start-up strategy has been validated together with the auto-resonant control explained in Section III by simulating the circuit in Fig. 6. The resulting waveforms are shown in Fig. 8. The simulation has been executed with the main coils used in [6] connected to a S-S compensation network tuned at $85\,\mathrm{kHz}$. Additionally, referring to Fig. 1, the other parameters selected are: $V_{in} = 48\,\mathrm{V}$, $t_{dead} = 140\,\mathrm{ns}$, and $R_L = 10\,\Omega$.

Fig. 8(a) shows that initially the RESET pin of the oscillator is set to high which enables the starting short pulses $p_{1,start}$ and $p_{2,start}$ in Fig. 8(b). This leads to the start of the control signals to the gate driver Q, $\overline{Q}$ in Fig. 8(c). Fig. 8(d) shows that the first current oscillation is detected by that the positive slope comparator because the signal V_+ changes from high to low. Therefore, the oscillator is automatically disabled by setting its RESET pin to low. However, the comparators cannot detect the second current oscillation because its amplitude is

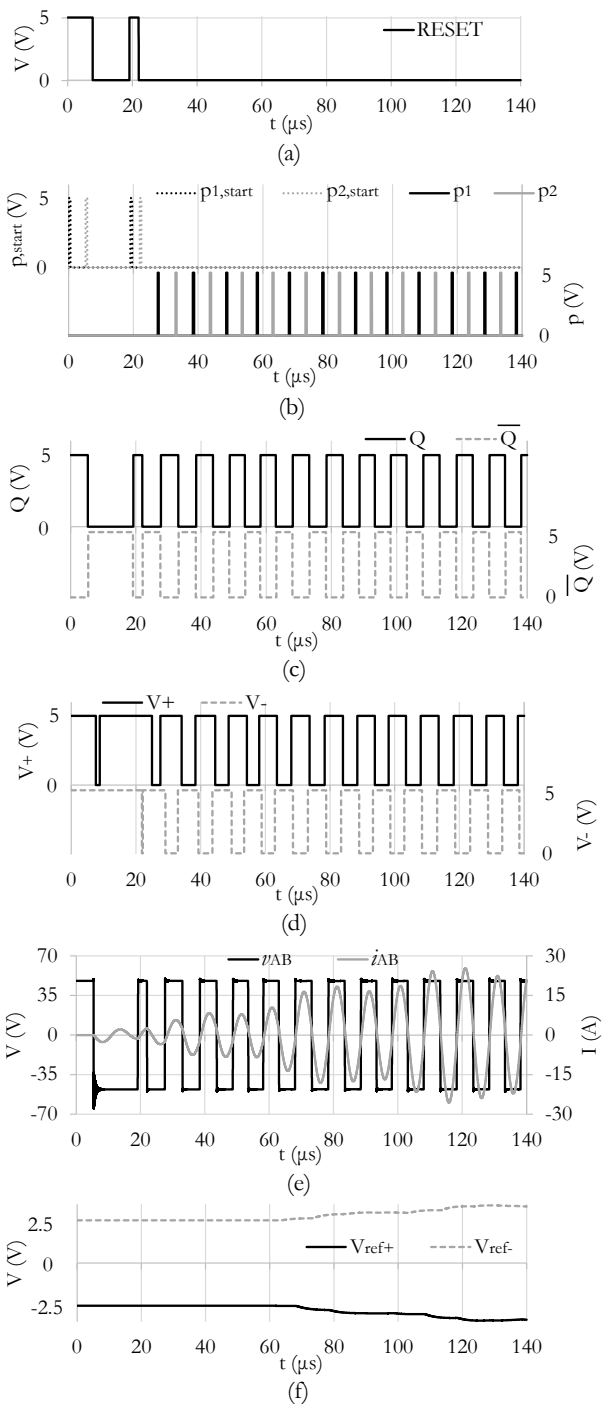

Fig. 8. Simulated waveforms of the start-up strategy described in Section IV. (a) Voltage to the RESET pin of the timed oscillator. (b) Starting short pulses $p_{1,start}$, $p_{2,start}$, and nominal short pulses p_1, p_2. (c) Control signals to the gate driver Q, $\overline{Q}$. (d) Output voltages V_+, V_- from the comparators. (e) Output voltage v_{AB} and current i_{AB} of the H-bridge inverter. (f) Voltage references V_{ref+}, V_{ref-} to perform the detection of i_{AB}.

not high enough. As a consequence, the oscillator is enabled again and two starting short pulses $p_{1,start}$ and $p_{2,start}$ are sent. After this, the nominal operation of the system starts. In Fig. 8(e), it is possible to notice that the ZVS turn-on is kept for the whole start-up transient even in the presence of current peaks higher than the 9 A steady-state peak current. This is realized by the auto-resonant control that adjusts the detection references V_{ref+}, V_{ref-}, as shown in Fig. 8(f).

V. Conclusion

This paper explains the concept of an auto-resonant control for the H-bridge inverter typically used in inductive power transfer applications. This concept consists of adapting the reference levels of the current's zero-crossing detection depending on the slope of the current at the zero-crossing. In this way, the operation is always adjusted to be close to the actual resonant frequency of the circuit, and the ZVS turn-on of the inverter is ensured at different operating conditions. By using the small-angle approximation, it has been proven mathematically that the reference levels for the zero-crossing detection depend on the derivative of the current around the zero-crossing. This justifies why the slope of the current is considered instead of its amplitude for the reference levels' computation. In particular, it has been decided to treat the positive and the negative-slope zero-crossing separately because of possible asymmetries in the current waveform and in delay times. The concept of auto-resonant control is explained with functional blocks and with qualitative operating waveforms. Finally, the strategy of the power transfer's start-up is also addressed. It has been proven with simulations that it is possible to use a timed oscillator to generate high-frequency pulses to excite a current flow in the inverter that makes the comparators work. As soon as the switching output from the comparators is sensed, the oscillator is disabled such that the power transfer can continue with its nominal operation.

References

[1] *J2954 RP: Wireless Power Transfer for Light-Duty Plug-In/ Electric Vehicles and Alignment Methodology*, SAE International Std., Apr. 2019.

[2] R. Steigerwald, "A comparison of half-bridge resonant converter topologies," *IEEE Transactions on Power Electronics*, 1988.

[3] B. Lu, W. Liu, Y. Liang, F. Lee, and J. van Wyk, "Optimal design methodology for llc resonant converter," in *Twenty-First Annual IEEE Applied Power Electronics Conference and Exposition (APEC)*, 2006.

[4] S. Li, W. Li, J. Deng, T. D. Nguyen, and C. C. Mi, "A double-sided lcc compensation network and its tuning method for wireless power transfer," *IEEE Transactions on Vehicular Technology*, 2015.

[5] T. Kan, T.-D. Nguyen, J. C. White, R. K. Malhan, and C. C. Mi, "A new integration method for an electric vehicle wireless charging system using lcc compensation topology: Analysis and design," *IEEE Transactions on Power Electronics*, 2017.

[6] F. Grazian, P. van Duijsen, T. B. Soeiro, and P. Bauer, "Advantages and tuning of zero voltage switching in a wireless power transfer system," in *IEEE PELS Workshop on Emerging Technologies: Wireless Power (WoW)*, 2019.

[7] F. Grazian, W. Shi, J. Dong, P. van Duijsen, T. B. Soeiro, and P. Bauer, "Survey on standards and regulations for wireless charging of electric vehicles," in *AEIT International Conference of Electrical and Electronic Technologies for Automotive (AEIT AUTOMOTIVE)*, 2019.

[8] H. L. Li, A. P. Hu, and G. A. Covic, "Fpga controlled high frequency resonant converter for contactless power transfer," in *IEEE Power Electronics Specialists Conference*, 2008.

[9] H. L. Li, A. P. Hu, G. A. Covic, and C. Tang, "A new primary power regulation method for contactless power transfer," in *IEEE International Conference on Industrial Technology*, 2009.

[10] W. Fu, B. Zhang, and D. Qiu, "Study on frequency-tracking wireless power transfer system by resonant coupling," in *IEEE 6th International Power Electronics and Motion Control Conference*, 2009.

[11] A. J. Moradewicz and M. P. Kazmierkowski, "Contactless energy transfer system with fpga-controlled resonant converter," *IEEE Transactions on Industrial Electronics*, 2010.